ADVANCED FUNCTIONAL MATERIALS
www.afm-journal.de

Industrial By-Products As a Novel Circular Source of Biocompatible Extracellular Vesicles

Cristina Lorca, Moisés Laparra, María Virtudes Céspedes, Laura Casaní, Sergi Florit, Mariona Jové, Natàlia Mota-Martorell, Elisabet Vilella, Xavier Gallart-Palau, and Aida Serra**

Extracellular vesicles (EVs) constitute an intricate system of molecular exchange that has recently gained tremendous interest. However, sustainable sources of safe biological EVs remain scarce and elusive. This study explores and defines the use of food industry by-products (BP) as a circular source of safe biocompatible EVs. Averaged diameter and molecular compositions indicate a large yield of exosomes and high abundancy of membrane lipids with signaling capacity in these vesicles. Complex proteomes mimicking those circulating in human blood plasma are also identified. Furthermore, BP-EVs do not show relevant cytotoxicity and display excellent oral and intravenous bioavailability together with specific organ targeting capacity. Collectively, it is believed that the novel findings reported here will open substantial venues for the use of BP as an optimal source of biocompatible nanovesicles in manifold applications of the biotechnological and biomedical fields.

1. Introduction

Spontaneous assembling of lipid hydrophilic heads and hydrophobic tails takes place in aqueous conditions by allowing the defiant acts of definition and differentiation, basis of any organismic existence. It is thus no wonder that bilayered lipid membranes remained largely and almost exclusively appreciated for these basic features, whereas their capacity to generate minute exocytic structures of cellular origin with outstanding properties was ignored.[1] These exocytic structures, currently known as extracellular vesicles (EVs), became once neglected as "cellular dust" or "cell debris."[1] Further multidisciplinary research, however, disclosed the weightiness of these particles at the time to protect specific cellular cargoes from extracellular hazards providing them with the most appropriate signaling molecules.[2] EVs, thus, constitute a highly complex intercellular communication mechanism based on extremely resilient and efficient lipid membranes, the inclusion of specific molecular cargoes, and the presence of preset membrane-embedded signaling molecules.[3] Additionally, these vesicles are shed and taken up by almost every cell type in the diverse kingdoms of life.[4]

Given these idiosyncratic properties, EVs have been proposed to perform essential functional role(s) in health and disease

C. Lorca, M. Laparra, A. Serra
IMDEA-Food Research Institute
Campus of International Excellence UAM+CSIC
Old Cantoblanco Hospital
8 Crta. Canto Blanco, Madrid 28049, Spain
E-mail: aida.serra@imdea.org

C. Lorca, X. Gallart-Palau
Biomedical Research Institute of Lleida Dr. Pifarré Foundation (IRBLLEIDA) – +Pec Proteomics Research Group (+PPRG) – Neuroscience Area – University Hospital Arnau de Vilanova (HUAV) – Health Campus
Psychology Department
University of Lleida
Lleida 25198, Spain
E-mail: xgallart@irblleida.cat

C. Lorca, X. Gallart-Palau, A. Serra
Proteored – Instituto de Salud Carlos III (ISCIII)
Lleida 25198, Spain

The ORCID identification number(s) for the author(s) of this article can be found under https://doi.org/10.1002/adfm.202202700.

DOI: 10.1002/adfm.202202700

M. V. Céspedes
Grup d'Oncologia ginecológica i peritoneal
Research Institute
Hospital de La Santa Creu I Sant Pau
Biomedical Research Institute Sant Pau (IIB-Sant Pau)
Barcelona 08041, Spain

L. Casaní, S. Florit
Research Institute Hospital de La Santa Creu I Sant Pau
Biomedical Research Institute Sant Pau (IIB-Sant Pau)
Barcelona 08041, Spain

M. Jové, N. Mota-Martorell
Department of Experimental Medicine
Lleida Biomedical Research Institute (IRB Lleida)
Lleida University (UdL)
Lleida 25198, Spain

E. Vilella
Hospital Universitari Institut Pere Mata
Reus, Tarragona 43204, Spain

E. Vilella
Institut d'Investigació Sanitària Pere Virgili (IISPV)
Reus, Tarragona 43204, Spain

E. Vilella, X. Gallart-Palau
Centro de investigación Biomédica en Red en Salud Mental CIBERSAM
Instituto de Salud Carlos III
Madrid 28029, Spain

conditions, some of which have already been uncovered.[5] Similarly, these vesicles have been identified as an optimal headstream of organic biocompatible nanocarriers with a growing interest, for their potential applications, within several areas of the bioeconomy and biomedical fields (i.e., food and supplement industries, biotech industries, pharmacy, etc.).[6] Although these vesicles display advantageous and compelling features as nanocarriers including low antigenicity, ability to trespass biological barriers, stable circulatory capacity, and organ tropism, the applicability of EVs as optimal nanocarriers still faces substantial challenges.[6] Among these safety, scalability and identification of biocompatible physicochemical features stand out as drawbacks.[7] This is in part due to the fact that the most researched sources of nanocarrier EVs are immortalized cell lines, a limiting source with significant concerns in terms of human safety and resource availability.[8] Similarly, the optimal progress of the EVs mimetics field, which consists of laboratory-based generation of artificial EVs and liposomes with biocompatible nanocarrier potentialities, faces substantial challenges based on the current available EVs sources.[9]

Foods are known to contain a vast population of EVs, naturally present and ingested by humans daily.[10] Presence of EVs in foods has been demonstrated in multiple sources, including milk and dairy products,[11] edible plants, plant-derived products, and fermented foods.[11] Furthermore, EVs from foods seem to tick the right boxes at the time to optimally perform as nanocarriers in terms of safety, biocompatibility, stability, and target specificity.[12] However, little is still known regarding appropriate sources of food EVs, optimal methods of obtainment, potential scalability, and advanced physicochemical properties of these vesicles.[12] Similarly, the use of food industry by-products (BPs) to obtain biocompatible EVs, to the best of our knowledge, has not been explored yet. These BPs and residues may become an optimal source of EVs with the collateral capacity to contribute to the progress of circular economy, a research priority worldwide.[13] Circular economy promotes reduction, recycling, and reusage of industrial waste in front of the end-of-life concept, improving overall sustainability. Food industries generate high amounts and a huge variety of BPs that have a negative environmental impact and high cost of management.[14] Thus, in this study, we have optimized and assessed different isolation methods to define EVs yield and scalability considering discarded food industry BPs as sources of circular EVs. Additionally, we have performed in-depth physicochemical characterization of the obtained food industry by-product-derived EVs (BP-EVs) with special emphasis on lipidome and proteome compositions. Finally, we have assessed the bioavailability, biodistribution, organ targeting capacity, and toxicity of these vesicles through in vivo and in vitro studies.

2. Results

2.1. Industry By-Products As a Novel Source of EVs

To define whether industry BPs can become a relevant source of potentially biocompatible EVs, four different and representative food industry-derived BPs were analyzed. Three of these BPs were supposed to exclusively contain EVs derived from plants and microorganisms (yeast and/or bacterial strains) (coded as BP1, BP3, and BP4), while BP2 was supposed to contain EVs derived from microorganisms and mammalian cells (further details on BP sources are provided in the Experimental Section). BP-EVs were initially isolated from their respective BP matrices by three different isolation methods: protein organic solvent precipitation (PROSPR), molecular weight cutoff (MWCO), and single-step size exclusion chromatography (SEC) as shown in **Figure 1**a. The selection of these methods was based on industrial scalability, methodological simplicity, lower execution costs, and standardization.

All tested isolation strategies provided substantial yields of BP-EVs from all analyzed samples (Figure 1b), in turn demonstrating the consistent presence of these vesicles in these sources. However, MWCO generated significantly improved yields on solid BP sources (BP3 and BP4) (Figure 1b-I–IV), while the difference on the quantity of EVs obtained among MWCO and the two other methods tested in liquid sources (BP1 and BP2) was not statistically significant (Figure 1b-I–IV). In addition, the facts that MWCO presents technical advantages, such as lack of requirement of organic solvents in its use and that it is easier to standardize and scale from an industrial perspective, were also taken into consideration. Hence, MWCO was chosen as the most optimal methodology to obtain BP-EVs in this context and thus this isolation method was used in all subsequent studies performed here, as depicted in Figure 1a.

Morphometric and ultrastructural characterization of the obtained BP-EVs indicated predominant particle sizes within the exosomal range for all tested BP-EVs isolation strategies (global averaged $\phi < 250$ nm) as indicated in Figure 1c and Figure S1, Supporting Information. However, collectively, BP1-EVs showed significantly larger averaged diameters (average ϕ 222.4 ± 22.7 nm) than BP2-EVs (average ϕ 132.7 ± 21.96 nm) and BP3-EVs (average ϕ 121.1 ± 8.545 nm) (Figure 1c). It was also observed that SEC isolated larger EVs in diameter from BP4 than the rest of isolation methods employed (Figure 1d). As previously described in other studies, different isolation methodologies tend to generate variation in the profiles of the obtained EVs.[15] Thus, the significant variations observed here regarding the use of SEC contributed to the election of the MWCO methodology as preferential, which allows the obtention of EV populations with diameters of closer compliance with the exosomal range for BP4 (Figure 1d). Finally, ultrastructural characterization of BP-EVs demonstrated that these vesicles present spherical morphology as shown in the representative micrographs in Figure 1e. Additionally, ultrastructural analysis confirmed low presence of contaminant particles in isolated BP-EVs preparations (Figure 1e).

2.2. Lipidome Compositions of BP-EVs

Lipids are essential components of EVs predominantly acting as structural components of the lipid bilayer membrane.[16] Here, we performed next-generation untargeted lipidomics to define the lipid compositions of the obtained BP-EVs. Identified molecules were initially classified in lipid families as shown

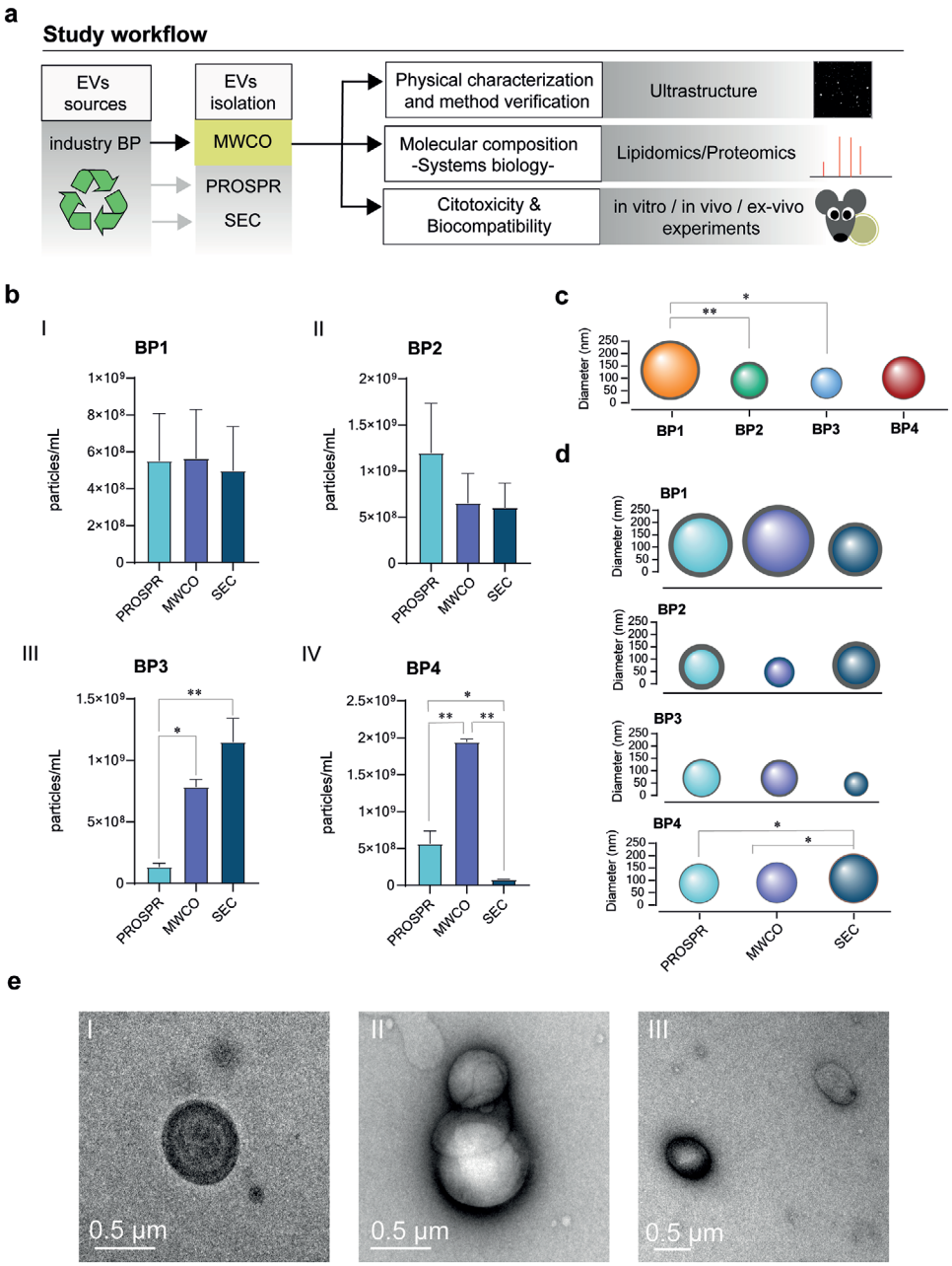

Figure 1. Experimental flow chart and morphometric characterization of BP-EVs isolated by PROSPR, MWCO, and SEC. a) Diagram that depicts the whole experimental flow chart procedures of the study. b) Particle concentrations detected by nanoparticle tracking analysis (NTA) in I. BP1-, II. BP2-, III. BP3- and IV. BP4-EVs using the three tested EVs isolation strategies. Reported data was based on ten sequential analyses (without any field nor parameter restrictions) from three independent experiments ($n = 3$). c) Averaged particle diameter of BP-EVs. Gray external line represents the standard deviation of the mean. d) Averaged particle diameter of BP-EVs depending on the EVs enrichment strategy used. Gray external line represents the standard deviation of the mean. e) Ultrastructural transmission electron microscopy micrographs of I. BP1-EVs and II-III. BP2-EVs. * Indicates significant differences at $p \leq 0.05$; ** Indicates significant differences at $p \leq 0.001$.

in **Figure 2**. Eight lipid families were commonly identified in all BP-EVs lipidomes, which included fatty acyls (FA), glycerophospholipids (GP), glycerolipids (GL), sphingolipids (SP), polyketides (PK), sterol lipids (ST), saccharolipids (SL), and prenol lipids (PR) (Figure 2a–h). GP was consistently identified as the most abundant lipid family in all BP-EVs metabolomes analyzed (Figure 2i); and the relative amounts of this lipid family were found more abundant in BP-EVs of plant/yeast origin (BP1) (Figure 2i). Significant differences on the relative amount of lipid families were also encountered for the GL species, which revealed higher abundancy in BP2 compared to BP1 and BP3 (Figure 2i).

In a related vein, multivariate partial least squares discriminant analysis (PLS-DA) of the molecular features identified

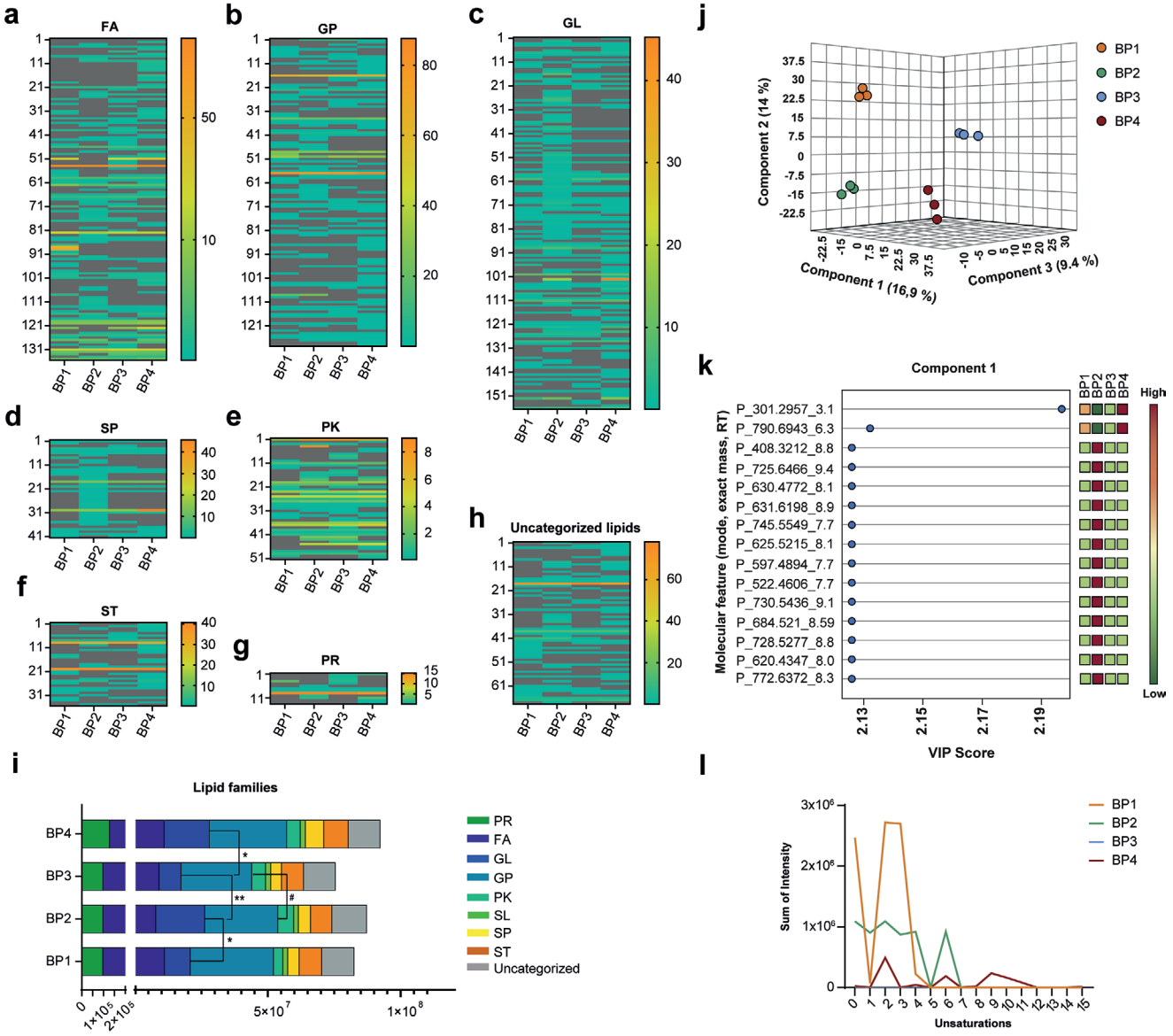

Figure 2. Categorization of lipid species from BP-EVs lipidomes. a–g) Heatmaps depicting the family categorization of lipid species identified from BP-EVs lipidomes, including fatty acyls (FA), glycerophospholipids (GP), glycerolipids (GL), sphingolipids (SP), polyketides (PK), sterol lipids (ST) and prenol lipids (PR). h) Heatmap that shows data from uncategorized lipid species in BP-EVs lipidomes. Species intensity in all heatmaps is expressed as relative intensity based on MS counts. i) Quantitation of lipid families identified in BP-EVs based on the sum of mass MS of the molecular species within every categorized lipid family. Multivariate partial least square discriminant analysis (PLS-DA) of the molecular features identified in BP-EVs lipidomes showing j) the BP-EVs sample separation according to lipidome compositions and k) important lipid features of component 1 based on Variable Importance in Projection (VIP) scores. k) Degree of unsaturation of lipids identified from the discriminative lipidome detected in every BP-EVs characterized. l) Quantifications are based on sum of intensities detected by LC-MS/MS. Significance was assessed by parametric ANOVA or by non-parametric Kruskal Wallis with a minimum significance level $p < 0.05$. Mean comparisons between BP-EVs groups were assessed by posthoc test. * Indicates significant differences at $p \leq 0.05$; ** Indicates significant differences at $p \leq 0.001$; # Indicates non-parametric significant differences at $p \leq 0.05$.

by liquid chromatography-mass spectrometry (LC-MS) demonstrated presence of a highly specific lipidome signature within each of the BP-EVs analyzed (Figure 2j). Of note, BP3 was the EVs subset with higher heterogenicity in the lipid compositions observed (Figure 2k). A total of 186 molecular features were differentially detected by liquid cromatography with tandem mass spectrometry (LC-MS/MS) (Table S2 and Dataset S1, Supporting Information). From these, 72 lipid species could be confidently validated (Tables S2 and S3, Supporting Information). Of note, cholesterol ester (CE), triacylglycerols (TAG), and cardiolipin (CL), all lipid molecules traditionally derived from contaminant particles in EVs preparations,[17–19] did not reach the significance threshold in any of the samples analyzed.

Finally, the degree of unsaturation of the differentially identified lipids in BP-EVs was also investigated (Figure 2l). BP1-EVs

lipidomes were enriched in saturated fatty acids (SFA), as well as in polyunsaturated fatty acids (PUFA) with low degrees of unsaturation. SFA were also present in BP2-EVs, together with monounsaturated (MUFA) and PUFA acids of up to 6 degrees of unsaturation (Figure 2l).

2.3. Proteome Characterization of BP-EVs

Unbiased discovery-driven proteomics to characterize the obtained BP-EVs proteome compositions was also performed by using next-generation 4D state-of-the-art technology,[20,21] BP1- and BP3-EVs were identified with richer proteomes (2372 ± 23 and 2625 ± 98 proteins, respectively) than BP2 and BP4 (243 ± 4 and 402 ± 113 proteins, respectively) (**Figure 3**a). Total proteins compared to total lipids in BP-EVs revealed that BP1-EVs contained the highest protein-to-lipid ratio whereas BP4-EVs displayed the lowest ratio (Figure 3b).

Subsequently, we evaluated whether the organism of origin of the identified BP-EVs proteomes modulated the proteome compositions (Figure 3c). These analyses revealed that 99% of BP1-EVs proteins came from yeast, specifically from *Saccharomyces cerevisiae* (Figure 3c). Thus, no EVs from plant origin were found in BP1-EVs proteomes. Similarly, BP2-EVs proteomes were identified with mammalian origin (*Bos taurus*) (in this particular case, proteins were also detected from the bacterial origin, though not consistently identified in at least three independent replicates and thus not considered) (Figure 3c). From BP3, which originally contains a complex mixture of lactic acid bacteria and yeast, 72% of identified EVs proteins were from the genus *Kamagataeibacter* (Figure 3c); whereas in BP4-EVs, 68% of the proteomes identified had plant origin (*Vitis vinifera)* and the remaining 32% possessed yeast-derived origin (Figure 3c). Of note, although microbial EVs proteins were less rich in complexity and diversity in BP4-EVs, these were far more abundant in the total proteomes of this BP compared to plant-derived EVs proteins as shown in Figure 3c.

2.4. BP-EVs Proteomes Differ from Previously Identified EVs Proteomes

We then investigated whether BP-EVs proteomes are alike to previously identified EVs proteomes curated in the EVs specialized databases Vesiclepedia and Exocarta.[22,23] Of note, only EVs from the mammal BP source (BP2) obtained a relevant match (76%) in these comparative analyses (Figure 3d). Rest of BP-EVs proteomes obtained matches lower than 3% (BP1 and BP4) or not match at all (BP3). Complete lists of uncategorized proteins generated in these comparative studies can be found in Dataset S3 (Supporting Information).

2.5. Diversity and Abundance of Membrane Proteins in BP-EVs

Membrane proteins represent lower portions of the total proteomes in BP1-, BP3-, and BP4-EVs (ratio membrane proteins/total proteome <0.5), with the exception of BP2-EVs, in which membrane proteins represent a higher >1 portion of the total proteomes (Figure 3e). Similarly, BP4-EVs showed a significantly higher ratio of membrane proteins compared to BP3-EVs (Figure 3e). The list of identified membrane proteins in each of the BP-EVs proteomes is included in Dataset S4 (Supporting Information). Relative quantification of the abundance of these identified BP-EVs membrane proteins revealed enolases as the family of EVs membrane proteins more ubiquitously present across the analyzed BP-EVs and more abundant together with immunity-related membrane proteins and glycoproteins (Figure 3f). Remarkably, although BP3 showed the lowest ratio of membrane proteins compared to rest of BP-EVs proteomes, the abundance level of a subset of specific membrane protein families was significantly higher in these BP-EVs including tetraspanins, apolipoproteins, glycoproteins, and immunity-related proteins (Figure 3f).

2.6. Similarities of BP-EVs with EVs in Human Plasma and in Consumed Foods

As expected, EVs from mammalian origin (BP2) displayed further complex proteome compositions in terms of biological processes, mirroring the proteome compositions in circulating human EVs (**Figure 4**a). On the contrary, plant and bacterial/yeast-derived EVs showed higher proportion of metabolic and cellular processes-related proteins compared to mammalian-derived EVs and scarce biological processes-related similarities with human circulating EVs (Figure 4a). Further analysis of EVs proteomes from mammal origin (BP-2) showed presence of proteins involved in key biological processes, such as proteins of the HIF-1-alpha regulatory pathway and MHC-I class-related proteins (Figure 4b). Similarly, in EVs from this BP, the proteins with modulatory capacity toward lipid digestion, lipid mobilization, and transport of lipids were more abundant (Figure 4b). Finally, these analyses also revealed significant enrichment of specific protein domains in BP2-EVs, highlighting the 2.31-fold enrichment in signal peptide-containing proteins as shown in Figure 4b.

In order to comparatively analyze BP-EVs with their food-derived counterparts, we analyzed BP2-EVs and BP4-EVs proteomes toward their respective previously reported bovine milk-derived EVs proteomes[24] and grape-derived EVs proteomes[10] (**Figure 5**). BP2 and BP4-EVs were selected here as representative EVs populations to be compared with their main food-derived EVs counterparts, given that the proteome composition of food-derived EVs isolated from the foods associated with the generation of BP2 and BP4 are well documented and easily available in front of food-derived EVs counterpart proteomes from the rest of BP-EVs sources analyzed. For BP2-EVs, 79% of the proteins consistently identified in our study were previously identified in bovine milk-derived EVs as shown in Figure 5a. In-depth ontology categorization of these common and uncommon proteins (Figure 5b,c) indicates no differences between BP2-EVs proteomes and milk EVs proteomes. Similarly, although grape-derived EVs proteomes have not previously been in-depth characterized,[10] comparative analyses between BP4-EVs and the partial available data on grape-derived EVs proteomes also demonstrated high similarities between these two EVs sources (Figure 5d and Table S4, Supporting Information).

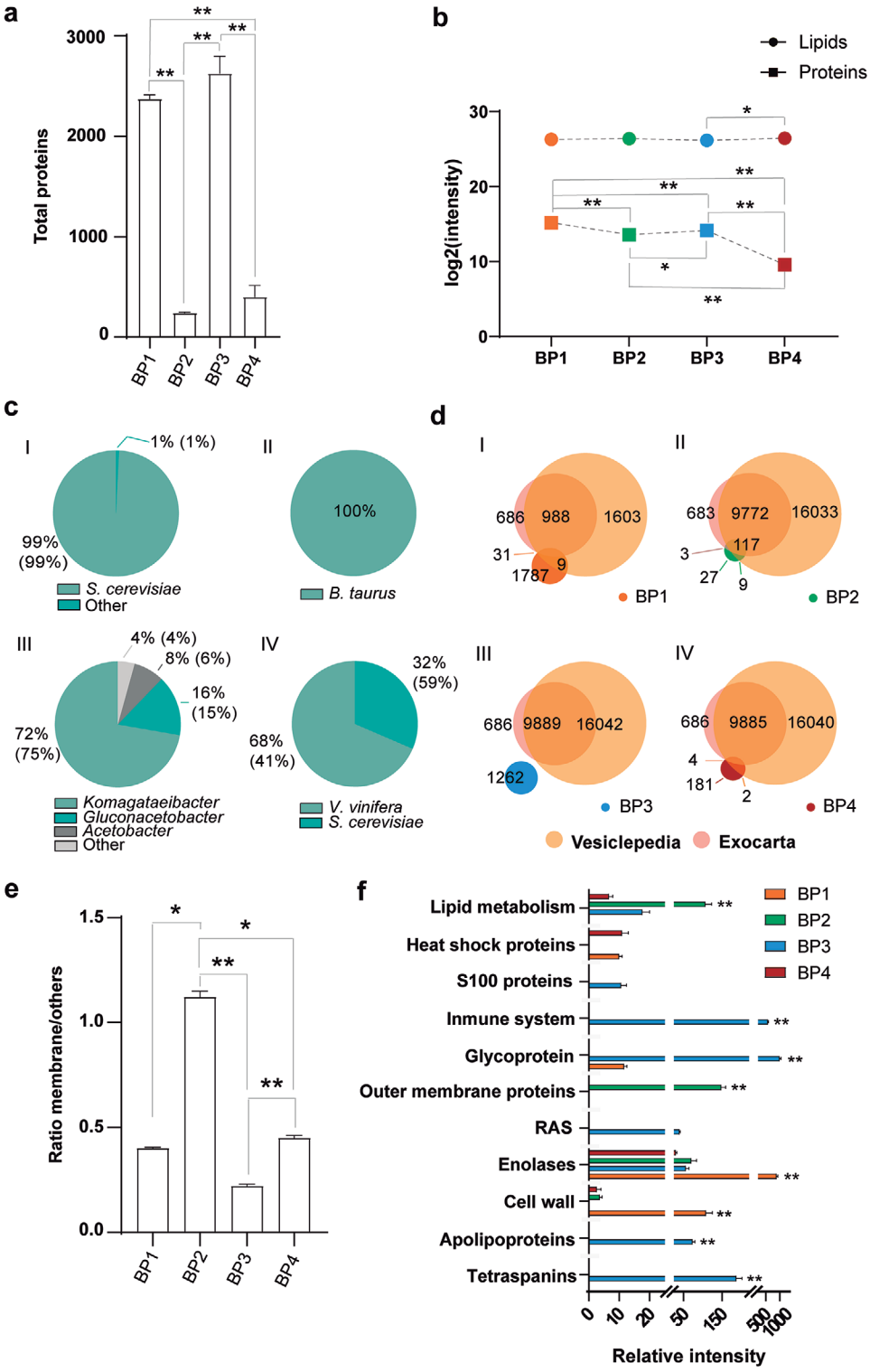

Figure 3. 4D proteomic characterization of BP-EVs by LC-MS/MS. a) Bar graph displaying the number of total proteins identified in each characterized BP-EVs proteome. b) Total intensity of lipids and proteins identified within each BP-EVs proteomes and metabolomes characterized. Total intensities were calculated based on the sum of intensities obtained from individual lipid identifications and the sum of spectral count of each protein in BP-EVs proteomes. Total intensity values were log2 transformed for a representative purpose. c) Parts of the whole graphics showing the percentage proportions that represent every organism in the total proteomes identified from: I. BP1-EVs, II. BP2-EVs, III. BP3-EVs and IV. BP4-EVs proteomes. Numbers in brackets indicate the percentage represented by each organism within BP-EVs proteomes. Only proteins consistently identified in at least three independent replicates are represented. d) Venn diagrams that depict overlapping between proteins identified in BP-EVs proteomes (I. BP1-EVs, II.

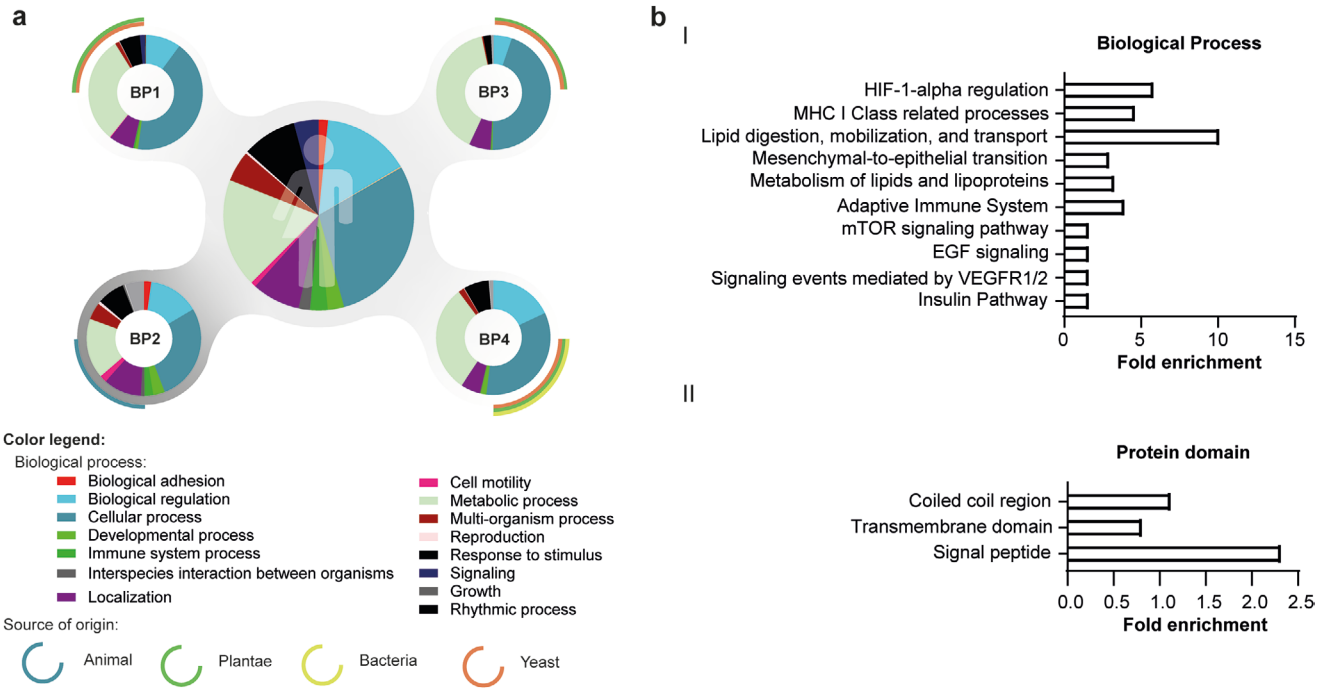

Figure 4. Comparative gene ontology (GO) analysis between BP-EVs proteomes and human blood plasma circulating EVs proteomes. a) Categorization of proteins according to the biological system to which they belong. Central circular graph depicts the categorization of proteins in circulating human EVs proteomes whereas external circular panels depict the categorization of proteins within each analyzed BP-EVs. Categories are distinguishable through different colors. The color of the external lines (located at the graph corners) indicates the source of origin of EVs. Stronger gray shades denote higher similarities between EVs proteomes. b) Detailed GO categorization of the most similar EVs proteomes identified between BP-EVs (BP-2) and human circulating EVs. Panel I. depicts categorization of common proteins and fold enrichment in the total BP-EVs proteome based on biological systems and II. depicts categorization of common proteins and fold enrichment in the total BP-EVs proteome based on protein domains.

2.7. In Vitro Assessment of BP-EVs Cytotoxicity

BP-EVs were assessed on their potential ability to exert significant harmful features on basic cell metabolism processes and cell viability. Representative BP-EVs from animal origin (BP-EVs-A) and from vegetal/yeast origin (BP-EVs-V) were used in these experiments as detailed in the Experimental section. Therefore, potential cell cytotoxicity of BP-EVs was investigated by using immortalized human colorectal Caco-2 cells by the implementation of the cytotoxicity assays neutral red (NR) and 3-(4,5-dimethylthiazol-2-yl)-2,5-diphenyltetrazolium bromide (MTT). As shown in **Figure 6**a, BP-EVs did not display significant decay on the absorbance obtained by NR uptake assay of lysosomal activity compared to negative (C_N) and positive controls (C_P), although some differences on NR assay results were found between the performed assays as shown in Figure 6a. Of note, an apparent although not significant decreasing tendency in NR absorbance for BP-EVs-V was also observed (Figure 6a), but this was not seconded by data obtained in the complementary assay MTT (Figure 6b). This fact indicates that further complex metabolic assays might also be useful at the time to better appreciate the cellular effects of these EVs, especially prior to their specific use in biomedical and biotechnological applications in humans. Similarly, cell viability assessed by the MTT assay did not show significant cytotoxicity exerted by BP-EVs compared to controls.

2.8. In Vivo and Ex Vivo Investigation of BP-EVs Bioavailability and Biodistribution

To scrutinize whether the obtained BP-EVs show relevant biocompatible abilities (e.g., targeting of specific organ tissues, circulation in biological fluids, ability to cross biological and cellular barriers, oral bioavailability, and postdigestion capacity) we performed in vivo whole-body noninvasive fluorescent imaging (FLI) experiments followed by ex vivo validation. Representative BP-EVs from BP-EVs-A and BP-EVs-V were used in these experiments as detailed in the Experimental section. Overall abdominal biodistribution of fluorescent labeled BP-EVs was predominantly observed at 4 h postoral administration (Figure 6c,d), time point when significant differences in whole-body fluorescent signal between BP-EVs-A and BP-EVs-V were also identified (Figure 6e). Of note, the observed FLI signaling

BP2-EVs, III. BP3-EVs and IV. BP4-EVs) and EVs proteins identified and curated in the EVs specialized databases Vesiclepedia and Exocarta. e) Graph bar that displays ratios of membrane proteins/other proteins within BP-EVs proteomes. These ratios were calculated based on data obtained from gene ontology analyses. f) Functional and molecular family categorizations of membrane proteins identified in BP-EVs proteomes including their relative abundance within proteomes. Significance was assessed by parametric ANOVA with a minimum significance level $p < 0.05$. Mean comparisons between groups were assessed by post-hoc test. * Indicates significant differences at $p \leq 0.05$; ** Indicates significant differences at $p \leq 0.001$.

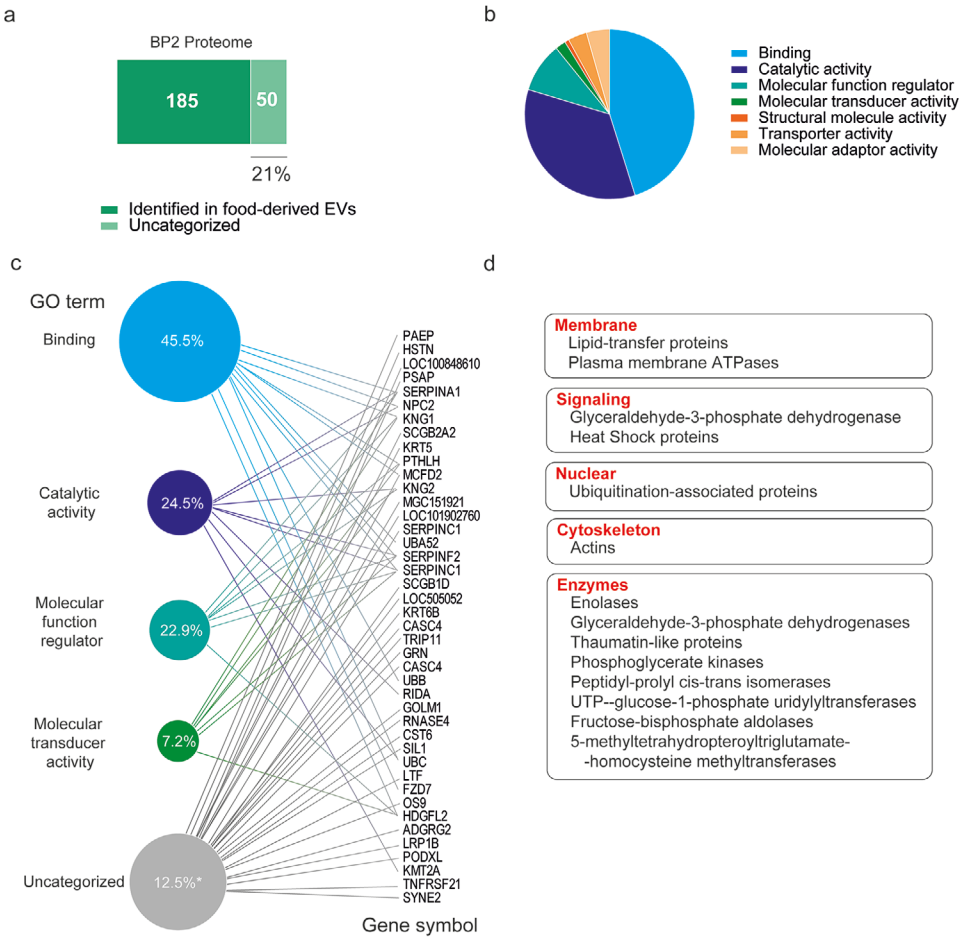

Figure 5. Comparative study of BP-EVs proteomes with their existing previously reported counterpart food-derived EVs proteomes. a) Number of common proteins and proteome proportions identified between BP2-EV proteomes and its food-derived EVs counterpart bovine milk. Proteomics data on bovine milk EVs were obtained from ref. [24]. b) Gene ontology (GO) analysis of BP2-EVs proteins that are common with proteins identified in bovine milk-derived EVs. Data were categorized based on molecular function. c) GO analysis of BP2-EVs proteins that were not previously reported as identified in bovine milk-derived EVs. GO data were categorized based on molecular function. d) GO analysis of BP4-EVs proteins that are common with proteins identified in grape-derived EVs. Data available on grape-derived EVs proteomes were obtained from ref. [10]. GO data were categorized based on molecular identity and cellular function.

differences within the thoracic region were not specifically analyzed due to the difficulties encountered to confidently attribute these to any specific organ within this region (Figure 6c,d). It was also observed that biodistribution signaling peaks were respectively and differentially found at 4 h and 24 h post-oral administration for BP-EVs-V and BP-EVs-A (Figure 6e). Of note, an apparent fluctuating behavior was observed regarding the FLI signal at the initial time-points analyzed, which was attributed to standard pixel intensity corrections.

Ex vivo organ validation at 25 h post-oral administration of BP-EVs, indicated differential targeting of these vesicles specifically in brain, liver, and bone tissues (Figure 6f–h). Although all analyzed BP-EVs sources demonstrated the ability to specifically target brain tissues by ≈20% of the total biodistributed vesicles (Figure 6h), only BP-EVs-V specifically targeted skeleton tissues (Figure 6f–h). Similarly, BP-EVs-A predominantly remained within hepatic tissues at 25 h post-oral administration (≈90% of total biodistributed vesicles) whereas only 60% of BP-EVs-V were trapped in the liver (Figure 6h). The rest of tissues analyzed that did not show significant changes in fluorescent biodistribution are shown in Figure S2 (Supporting Information).

Finally, data from the experiments performed to compare the biodistribution capacity of BP-EVs based on the via of administration (tail-intravenous versus oral), which indicated excellent oral bioavailability of BP-EVs-A and BP-EVs-V for both analyzed BP sources, were included in Figure S3a–c (Supporting Information). Higher hepatic accumulation of BP-EVs was observed following to tail-intravenous administration (i.v.) compared to oral administration (Figure S3d,e, Supporting Information), therefore oral administration was revealed as the most optimal administration via to achieve broader whole-body biodistribution of BP-EVs (Figure S3d,e, Supporting Information).

3. Discussion

In the present work, to the best of our knowledge, we provide first vast evidence that industry BPs can become a relevant

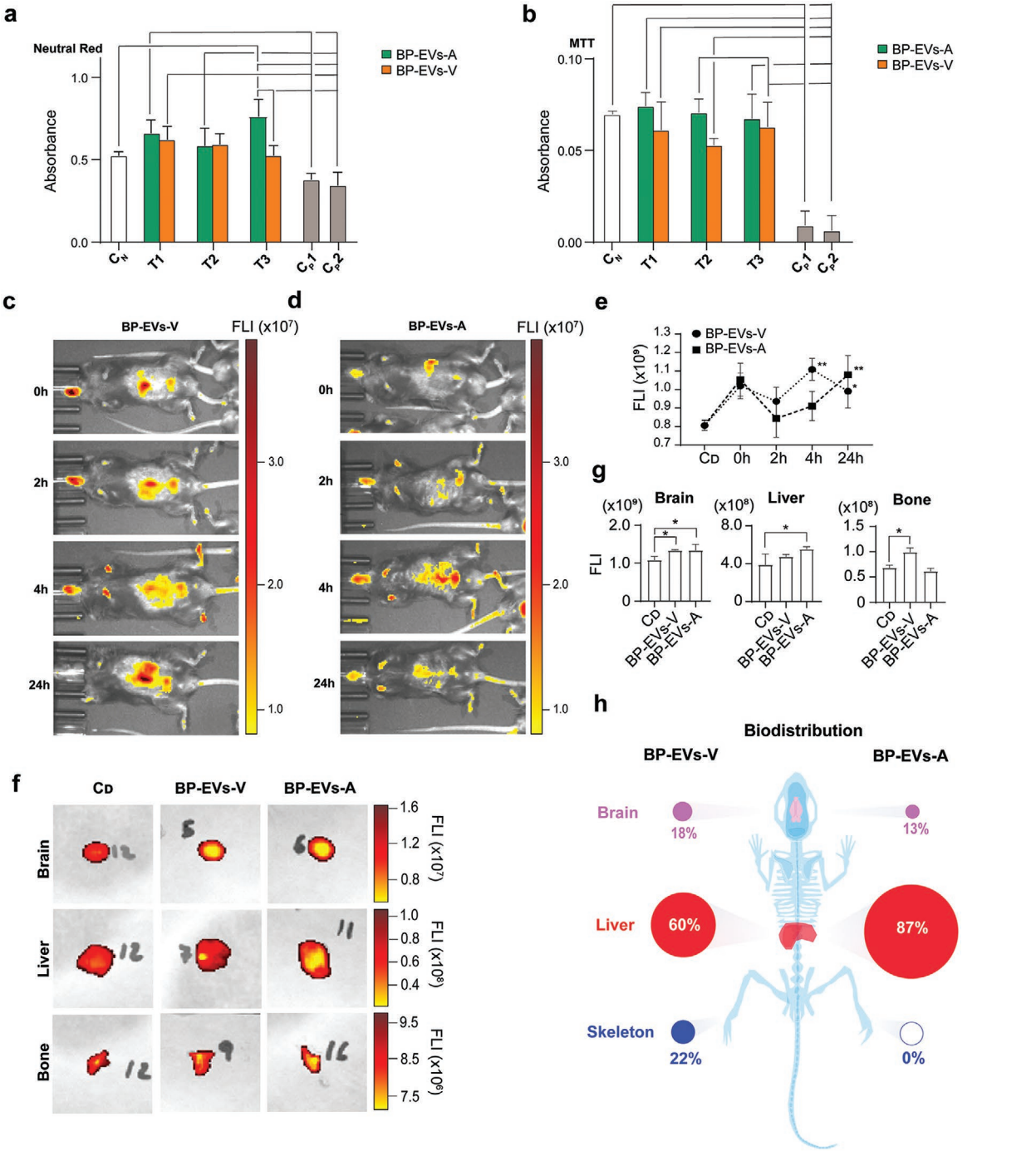

Figure 6. Biocompatibility analysis of BP-EVs by assessing in vitro cytotoxicity, in vivo biodistribution, and organ targeting capacity. In vitro cytotoxicity was assessed in Caco-2 cells seeded in 96-well cell plate at a cell density of 15 000 cells per well treated with different concentrations of BP-EVs of animal origin (BP-EVs-A) and vegetable/yeast origin (BP-EVs-V) (Treatment 1 (T1): 10^8 particles per mL^{-1}, Treatment 2 (T2): 10^9 particles mL^{-1} and Treatment 3 (T3): 10^{10} particles mL^{-1}) by a) Neutral Red uptake assay of lysosomal activity and b) cell viability MTT assay. The negative control was performed treating cells with PBS (C_N: 50%) and the positive control (C_P) treating cells with two concentrations of DMSO (C_P1: 10% and C_P2: 30%). Continuous lines between bars indicate significant differences. Whole-body noninvasive monitoring of the biodistribution of fluorescent. c) BP-EVs-A and d) BP-EVs-V at 0, 2, 4, and 24 h upon oral administration. FLI corresponds to fluorescent intensity expressed in radiant efficiency. e) Total whole-body accumulation of fluorescent BP-EVs at 0, 2, 4, and 24 h quantified by measurements of FLI. f) Ex vivo tissue fluorescent imaging at 25 h post-oral administration of BP-EVs-A or BP-EVs-V. g) Total tissue accumulation was quantified by the measurement of FLI. Only tissues that showed significant differences compared to the positive control corresponding to animals treated with the fluorescent dye (C_D) are displayed. Results from other investigated tissues are shown in Figure S3 (Supporting Information). h) Relative biodistribution of BP-EVs-A and BP-EVs-V at 25 h post-oral administration, considering accumulation in tissues that showed significant differences compared to C_D. Significance was assessed by parametric ANOVA with a minimum significance level $p < 0.05$. Mean comparisons between BP-EVs groups were assessed by post-hoc test. * Indicates significant differences at $p \leq 0.05$; ** Indicates significant differences at $p \leq 0.001$.

source of EVs, predominantly of exosomes, with a global average diameter <170 nm and expressing most of the relevant molecular markers associated with this specific subfamily of EVs, including ESCRT machinery tetraspanins and other multivesicular bodies-related proteins.[22,23,25] The exploitation of industry BPs as a source of EVs as we investigate here, goes paired with the use of an optimized, scalable, and efficient EVs isolation strategy.[12] In this study, PROSPR, MWCO, and SEC were investigated as they share common basic features, such as scalability and lowered costs of execution.[12] Optimized MWCO displayed the most efficient and simple way to obtain BP-EVs with improved yields even in solid BP sources. Furthermore, we believe that this isolation strategy can be easily industrially adapted, based on our reported parameters, through optimization of its available industrial sibling tangential flow filtration.

Our analyses also revealed that BP-EVs contain all the innate grandeur of food EVs with the important additions of wide availability, significantly reduced cost of obtention and higher sustainability. Morphologically, BP-EVs do not differ significantly from their food EVs counterparts. The average diameter of BP2-EVs was consistent with those previously identified in bovine milk,[26] whereas the average diameter of BP4-EVs was also in consonance with EVs isolated from grape,[27] the unique BPs that possess previously reported data from counterpart food-derived EVs. In terms of biochemistry, BP-EVs lipidomes revealed GP, GL, and FA as the lipid families more abundantly present. Richness in phospholipid families, as identified here, is a common feature of biological eukaryotic membranes[18] and a typical feature of EVs from bacteria,[28] plants, fungus,[29] and human origins.[3] Moderate enrichment in ceramides (Cer), a family of lipids which its presence is linked to biogenesis of exosomes,[30] was also detected in BP-EVs. Similarly, abundance of certain lipid families in EVs is associated with their tumorigenic origin[19] and a deleterious impact on recipient cells.[31] Thus, it has been shown that the families of lipids ST, SP, and GP are typically enriched in EVs of tumorigenic origin[19] while FA, GL, and PR abound in EVs of nontumorigenic origin. Our obtained results were consistent with these previous findings, as we found that BP-EVs preparations were significantly enriched in FA, GL, and PR lipids, fact that reinforces the links between BP-EVs and their food-derived counterparts and their capacity to avoid potential safety concerns. Exosomes have also been associated with presence of desaturated molecular species in their bilayer membranes,[30] finding also consistent with our lipidome data from BP-EVs. Additionally, analysis of the degree of saturation of lipids in these vesicles revealed that in general terms BP-EVs are enriched in PUFAs with low degree of unsaturations; what confers their membranes with manifold and dynamic cell signaling abilities[32] that may be specifically investigated in further studies based on the data generated here. In a related vein, study of BP-EVs proteomes indicated that these vesicles are enriched in specific coiled coil domain-containing proteins,[33] surface receptors, and cell adherent factors, which based on our results identifies BP-EVs from mammal origin as highly similar to EVs circulating in the human body. Enolases or GPI-anchoring proteins, among others, were the most ubiquitous proteins present in all BP-EVs characterized here. These molecules have previously been involved in quality control of EVs preparations and may act as indicators of EVs bioactive capacity.[34] Our proteome data also indicates that BP-EVs are predominantly produced by probiotic microbiota strains, such as lactic acid bacteria,[35] which associates our uncovered vesicles with immune system reinforcement as opposed to proinflammatory features generally associated with commensal or symbiotic bacterial strain-generated EVs.[36,37]

Intact whole body FLI and ex vivo studies, as performed here, serve as proof of concept of the biocompatible nature of BP-EVs and their ability to act as preferential organic nanocarriers. Furthermore, our in vitro assays with human colorectal Caco-2 cells indicated that BP-EVs did not exert relevant harmful features for cell metabolism nor cytotoxicity, even at higher dosages. FLI experiments demonstrated excellent time-linked biodistribution of i.v. and orally administered BP-EVs and specific organ targeting capacity of these vesicles. Based on the recent systematic review performed by Chamley and co-workers,[38] the peak of administered BP-EVs between 2 and 24 h in intact animals was also observed here in abdominal regions that may correspond to the liver.[38] However, we did not observe any attributable peak within thoracic regions matching the lungs. Similarly, BP-EVs signal was detected in head regions that correspond to the brain within all-time intervals measured from 2 h. These findings are consistent with previous reports on biodistribution of exosomes administered preferentially intravenously,[38] though, we also demonstrate here that orally administered BP-EVs display highly similar biodistribution patterns. Furthermore, as a novelty of this study, we confirmed by ex vivo FLI that BP-EVs remain in brain tissues beyond the timepoint of 24 h, and that these vesicles preferentially target bone, brain, and liver tissues. Consistent with previous reports,[39] distinct EVs sources display differential biodistribution patterns and particular tissue or cell targeting properties. These tissue targeting discrepancies are caused by specific EVs membrane proteins and lipids that require specific elucidation on the basis of previously performed proteome- and lipidome-wide characterizations, as those reported in this study, that should pave the way for further studies in the field.

4. Conclusions

EVs have vastly demonstrated outstanding potential as next-generation delivery nanocarriers in manifold biotechnological and biomedical applications. However, current sources of EVs present substantial challenges including availability, cost, and safety as the most relevant. Here, we demonstrate for the first time the presence of EVs in food industry by-products. These food industry by-products, paired as detailed with an optimized and scalable method of EVs isolation, can become a sustainable source of EVs that surpasses any current existing source. Similarly, BP-EVs show exosomal predominance, outstanding biocompatible features, capacity to trespass biological barriers, and excellent oral bioavailability. These features, extensively detailed in this work, place BP-EVs as an optimal source of next-generation delivery nanocarriers with prospective manifold applications in biotechnology and biomedicine and extraordinary influence on the current and prospective translational mainstreams of the field.

5. Experimental Section

Reagents: Caco-2 cells were obtained from DSMZ (Braunschweig, Germany). All reagents were purchased from Sigma-Aldrich (St. Louis, MO) unless otherwise specified. Sequencing-grade modified trypsin was obtained from Promega (Madison, WI).

Food Industry By Products: Four different fermented food industry BP (FFIBP) were used in this study as potential source of circular EVs: i) brewer spend yeast derived from the beer fermentation production, generously provided by Mahou San Miguel brewery (Alovera, Spain); ii) whey from unbranded plain yogurt purchased in a local supermarket; iii) symbiotic culture of bacteria and yeast (SCOBY) derived from the production of tea fermented drink (Kombucha) on-line purchased from Kirandia—Ingenio Corporate Group, S.L. (Madrid, Spain) and iv) fermented wine pomace from red grapes derived from the wine fermentation production, generously provided by Castell del Remei winery (Penelles, Spain).

Preparation of Food Industry By-Products Prior EVs Isolation: Prior to EVs isolation, BP were pre-processed as follows: brewer spend yeast (≈15 mL) was centrifuged at 10 000 × *g*, 30 min at 5 °C to obtain by-product 1 (BP1); Whey from plain yogurt (BP2) was obtained by centrifugation of commercial yogurt (≈25 mL) at 10 000 × *g*, 30 min at 5 °C of plain; SCOBY derived from the production of kombucha (BP3) and fermented wine pomace (BP4) were obtained by respective manual homogenization of 3 g each of SCOBY and wine pomace in 15 mL of PBS by using a glass Dounce homogenizer. All pre-processed BPs were stored −80 °C until further use.

EVs Isolation Methods: Three different industrially scalable methods were selected based on scientific literature and tested for enrichment of BP-EVs. All experiments were performed in independent batches per triplicate.

Protein Organic Solvent Precipitation: PROSPR was applied to obtain EVs from 4 mL of BP1-4 as previously described.[3,40] Briefly, BP was mixed with four volumes of chilled acetone (−20 °C), the mixture was vortexed and centrifuged for <1 min at 5000 × *g*. The supernatant containing EVs was concentrated in a vacuum concentrator till near dryness (Concentrator Plus, Eppendorf AG, Hamburg, Germany). Concentrated BPs-EVs samples were stored at −80 °C until further analysis.

Single-Step Size Exclusion chromatography: Isolation of BP-EVs by SEC was performed as previously reported by Böing et al.,[41] with minor modifications. Briefly, Sepharose CL-2B was washed with 0.32% trisodium citrate prepared in PBS (0.22 µm filtered) by spinning 10 mL of Sepharose at 4500 × *g*, 5 °C for 5 min. Supernatant was removed, 6 mL of PBS was added, and the mixtures were vortexed for 1 min followed by centrifugation 4500 × *g* at 4 °C for 5 min. Sepharose was then three times washed. The tip of a 10 mL plastic medical HENKE-JECT syringe (Henke Sass Wolf GmbH, Tuttlingen, Germany) was stuffed with commercial nylon stocking (20 denier HM, Västerås, Sweden). Subsequently, the suspension of Sepharose in PBS was filled and stacked in the syringe by creating an in-house made column of approximately 6 cm height. For EVs enrichment by single-step SEC, 4 mL of preprocessed BPs sample was loaded into the column. Elution was performed with a PBS solution including 0.32% citrate (pH 7.4, 0.22 µm filtered). Eluates were then collected in three sequential steps by using 4 mL in each step. Based on the strategy designed by Böing, et al.,[41] BP-EVs were eluted in the second fraction. Presence of BP-EVs was experimentally confirmed by Nanoparticle Tracking Analysis (NTA). SEC isolated BP-EVs samples were finally stored at −80 °C till further use.

Molecular Weight Cut-Off: Isolation of BP-EVs by MWCO was performed from 3 mL of pre-processed BP by using Vivaspin PES 300 kDa MWCO spin-filters. Spin-filters were centrifuged at 6000 × *g* for 35 min at 4 °C. After initial centrifugation of 3 mL of BPs sample, the sample remaining in the upper side of the MWCO membrane was washed twice with 10 mL of PBS and spin-filter was centrifuged again using the same conditions. Concentrated BP-EVs sample remaining in the upper side of the filter was collected and stored at −80 °C for further downstream analysis.

Nanoparticle Tracking Analysis: Isolated BP-EVs, as stated above, were subjected to extensive volumetric and morphometric characterization by NTA. NTA was done as previously described with minor modifications.[42] Here, NTA analysis of BP-EVs was performed using a ZetaView BASIC NTA—Nanoparticle Tracking Video Microscope PMX-120 operated with ZetaView software (version 8.05.11) (Particle-Metrix, Ammersee, Germany). For each BP-EVs sample analyzed, 10 independent readings covering the entire sample run were achieved. BP-EVs samples were diluted to 1/1000 prior to NTA analysis in PBS to reduce the number of particles within the observational field at <200 per image.

Ultrastructural Analysis of BP-EVs: Isolated BP-EVs preparations from the representative sources (BP1 and BP2) were mounted on Cu-Formvar-Carbon grids, let for 20 min at RT, washed in distilled water, and fixed by 1% glutaraldehyde in PBS for 5 min. Subsequently, samples were stained with uranyl-oxalate solution for 5 min. Finally, BP-EVs samples were embedded by methyl-cellulose-uranyl-oxalate and dried for permanent preservation. Electron micrographs were collected using a Jeol Jem1010 electron microscopy. at a voltage of 80 kV.

Characterization of BP-EVs by Lipidomics—BP-EVs Lipid extraction: For lipid extraction, 5 µL (≈2.5×10^5 particles) of concentrated BP-EVs were mixed with 5 µL of milliQ water and 20 µL of ice-cold methanol. Samples were vigorously shaken by vortexing for 2 min and then, 250 µL of methyl tert-butyl ether (MTBE), were added. Samples were immersed in a water bath (ATU Ultrasonidos, Valencia, Spain) with an ultrasound frequency and power of 40 KHz and 100 W, respectively, at 10 °C for 30 min. Then, 25 µL of milliQ water was added to the mixture, and organic phase was separated by centrifugation (1400 *g*) at 10 °C for 10 min.[43] BP-EVs-derived lipid extracts, contained in the upper phase, were collected and subjected to liquid chromatography electrospray ionization quadrupole time-of-flight mass spectrometry (LC-ESI-Q-TOF MS/MS). Internal isotopically labeled lipid standards for each class were used for signal normalization.[44] Stock solutions were prepared by dissolving lipid standards in MTBE at a concentration of 1 mg mL^{-1}, and working solutions were diluted to 2.5 µg mL^{-1} in MTBE.

Nontargeted Lipidomics LC-MS: BP-EVs-derived lipid extracts were analyzed following a previously published method.[45] For LC-Q-TOF-based lipid molecular species analysis, BP-EVs-derived lipid extracts were subjected to LC-MS using a UPLC 1290 series coupled to ESI-Q-TOF MS/MS 6545 (Agilent Technologies, Barcelona, Spain). Sample compartment of the UHPLC was refrigerated at 4 °C and for each sample, 10 µL of FFIBP EVs-derived lipid extract were applied onto 1.8 µm particle 100 × 2.1 mm id Waters Acquity HSS T3 column (Waters, Milford, MA) heated at 55 °C. The flow rate was 400 µL min^{-1} with solvent A composed of 10×10^{-3} M ammonium acetate in acetonitrile–water (40:60, v/v) and solvent B composed of 10×10^{-3} M ammonium acetate in acetonitrile–isopropanol (10:90, v/v). The gradient started at 40% of mobile phase B and reached 100% B in 10 min and held for 2 min. Finally, the system was switched back to 60% of mobile phase B and was equilibrated for 3 min. Duplicate runs of the samples were performed to collect positive and negative electrospray ionized lipid species in TOF mode, operated in full-scan at 100 to 3000 m/z in an extended dynamic range (2 GHz), using N2 as nebulizer gas (5 L min^{-1}, 350 °C). The capillary voltage was set at 3500 V with a scan rate of 1 scan s^{-1}. Continuous infusion using a double spray with masses 121.050873, 922.009798 (positive ion mode) and 119.036320, 966.000725 (negative ion mode) was used for in-run calibration of the mass spectrometer instrument.[46]

Nontargeted Lipidomics Bioinformatics and Data Analysis: MassHunter Qualitative Analysis Software (Agilent Technologies, Barcelona, Spain) was used to obtain the molecular features of the samples, representing different comigrating ionic species of a given molecular entity using the Molecular Feature Extractor (MFE) algorithm (Agilent Technologies, Barcelona, Spain). MassHunter Mass Profiler Professional Software (Agilent Technologies, Barcelona, Spain) and Metabolanalyst Software were used to perform a nontargeted metabolomics and lipidomic analysis over the extracted features. Only those features with a minimum of 2 ions were selected. After that, the molecular characteristics in the samples were aligned using a retention time window of 0.1% ± 0.25 min and 30.0 ppm ± 2.0 mDa. Only features found in at least 70% of the

QC samples were considered to correct for individual bias and signal was corrected using LOESS approach. Multivariate statistics (partial least-squares discriminant analysis (PLS-DA)) were performed using Metaboanalyst software. Features representing significant differences by univariate statistics ANOVA ($p < 0.05$), defined by exact mass and retention time, were reported. An initial tentative classification into lipid families of the molecular features present consistently in three replicates was performed using CEU Mass Mediator v.3.0 (accuracy < 10 ppm). Identities of interest were also searched against the HMDB (accuracy < 30 ppm) and LIPID MAPS (accuracy < 20 ppm) databases. The identities obtained were compared with the retention time of the authentic standards added. Finally, identities were confirmed by MS/MS by checking the MS/MS spectrums using LipidBlast software and LipidMatch, a R-based tool for lipid identification.

Proteomics Characterization of EVs—In Solution Digestion of BP-Derived EVs Proteomes: BP-EVs (≈4.2×10^7 particles) were processed for vesicle lysis and denaturalization of proteins by dissolution in 16 M urea prepared in 100×10^{-3} M ammonium bicarbonate. After 20 min of mixture incubation at room temperature, samples were diluted with HPLC-grade water to 8 M urea. Protein amount in each analyzed sample was quantified by bicinchoninic acid (BCA) assay. BP-EVs constituent proteins were then digested for shotgun proteomics as previously described,[47] with little modifications. Briefly, solubilized BP-EVs proteomes were reduced with 20×10^{-3} M dithiothreitol at 30 °C for 3 h and alkylated with 40×10^{-3} M iodoacetamide for 1 h at room temperature prevented from the light. Trypsin digestion was subsequently performed overnight at 37 °C by adding a 20 µg of sequencing-grade trypsin to the samples and subsequently quenched by addition of a final concentration of 0.5% formic acid (FA). Tryptic digested peptidomes were then desalted through 100 mg C18 Sep-pack cartridge (Waters, Milford, MA). Elution was performed using 1 mL of 75% acetonitrile, 0.1% FA. Eluates were dried using a vacuum concentrator and stored at −20 °C till further proteomics analysis.

Liquid Chromatography Tandem-Mass Spectrometry of BP-EV Proteomes: Desalted BP-EVs peptidomes were resuspended in 0.1% FA prior to LC-MS/MS analysis by using a nanoElute liquid chromatograph (Bruker Daltonics, MA, USA) at 300 nL min^{-1} and ran using a 60 min linear gradient of 3–45% ACN. The nanoElute liquid chromatograph was online coupled to a state-of-the-art timsTOF Pro mass spectrometer (Bruker Daltonics, MA, USA) using parallel accumulation—serial fragmentation (PASEF) data acquisition.

Proteomics Bioinformatics and Data Analysis: Analysis of BP-EVs obtained proteomics raw data was carried out in the specialized bioinformatics suite software PEAKS Studio X, allowing a precursor ion tolerance of 10 ppm and a fragment ion tolerance of 0.05 Da. In-house databases were created by combining the existent proteome available in National Center for Biotechnology Information (NCBI) from all possible organisms present in every BP sample based on existent literature. Detailed information about organisms considered in each database is included in Table S1 (Supporting Information). Carbamidomethyl of Cys was set as fixed modification during the proteomics bioinformatics database search. PTM algorithm available in PEAKS Studio software was used for the identification of protein post-translational modifications. FDR < 1% was established for protein identification in all samples and trypsin was set as a proteolytic enzyme. Data were exported to Microsoft Excel CSV files and in-house generated macros were used for protein quantification analyses. Gene ontology (GO) analysis for comparison of BP-EVs proteomes with human circulating EVs proteomes was performed with PANTHER version 16.0. List of proteins identified from human circulating EVs isolated by ultracentrifugation with sucrose cushion was obtained from the previously published work of the authors.[40] Further categorization of membrane proteins was performed by using in-house macro software or by performing functional enrichment analysis in the open-source specialized software FunRich version 3.1.4.

Cell Toxicity Assessment by In Vitro Assays—Cell Culture: Caco-2 cells were cultured in Dulbecco's modified Eagle's medium (Biowest) complemented with 1% fetal bovine serum (Biowest), non-essential amino acids, sodium pyruvate, and HEPES buffer solution (Biowest), at 37 °C with 5% CO_2.

MTT and Neutral Red Assays: Caco-2 cells were cultured in P96 well plates at 15.000 cells per well with a volume of 100 µL. 24 h after culturing, the medium was removed and BP-EVs were added at three different concentrations: Treatment 1 (T1): 10^8 particles mL^{-1}, Treatment 2 (T2) 10^9 particles mL^{-1} and Treatment 3 (T3): 10^{10} particles mL^{-1} prepared in 50 µL PBS and 50 µL of complete medium without serum. The negative control was performed treating cells with PBS (C_N: 50%) and the positive control was performed treating cells with two concentrations of DMSO (C_P1: 10% and C_P2: 30% diluted in PBS). Cells were incubated for 24 h and after the incubation period, 3-(4,5-dimethylthiazol-2-yl)-2,5-diphenyltetrazolium bromide (MTT) and Neutral Red (NR) assays were performed. Briefly, the medium was retired and MTT/NR solutions (1:10 dilution in PBS) were added and incubated for 40 min at 37 °C with 5% CO_2. Cells were then washed with PBS and distaining solutions (10% sodium dodecyl sulfate in 0.01 M HC1 for MTT and 50% ethanol 96%, 49% deionized water, 1% glacial acetic acid for NR) were added. Absorbance was measured at 590 and 540 nm respectively using a spectrophotometer VICTOR Nivo Multimode Microplate Reader.

Fluorescent Imaging Monitoring of BP-EVs Bioavailability and Biodistribution In Vivo—Animals: All in vivo experiments were carried out at the Animal Experimental Service (SEA) of the Institut de Recerca de l'Hospital de la. Santa Creu i Sant Pau. All the in vivo procedures were approved by the Hospital de Sant Pau and Hospital Vall d'Hebron Animal Ethics Committees (Approval Ref #10234; date of approval 20th March 2019; Project *"Evaluation of nanoconjugates for directed therapy in murine models"*) and performed according to and in strict accordance with the International Guiding Principles for Animal Research.

Fluorescent Labeling of BP-EVs: Fluorescent labeled BP-EVs were prepared fresh prior to the in vivo study. BP-EVs resuspended in PBS were labeled with 1×10^{-6} M of Vybrant DiD Cell-Labeling Solution (Invitrogen, Waltham, USA) at 37 °C for 20 min. Subsequently, excess of dye was removed by filtration using a 10 kDa MWCO filters following manufacturer's instructions. Passed-through liquid containing the unbound dye and fluorescent-labeled BP-EVs were collected.

In Vivo Administration of Fluorescent-Labeled BP-EVs: 10-weeks old C57BL/6NT mice ($n = 16$) were housed in cages on a 12 h dark/light cycle at stable temperature (21 °C) with water provided ad libitum and fed with standard commercial chow for a minimum of 2 weeks (adaptation period) before starting the study. Mice were maintained in fasting conditions 16 h before the experimental procedure. Mice were treated with ≈3×10^9 particles suspended in 200 µL of PBS administered orally (oral) or by tail-intravenous injection (i.v.). BP1 and BP2 were chosen in this experiment as representative BP-EVs from animal (BP-EVs-A) and yeast/vegetal (BP-EVs-V) sources, respectively. Two different controls were also carried out; a control of the dye where the same amount of dye was mixed with PBS (C_D) and a negative control where PBS were administered (C_N).

In Vivo and Ex Vivo Whole-Body Biodistribution of Fluorescent-Labeled BP-EVs: The oral bioavailability and whole-body biodistribution of fluorescent-labeled BP-EVs were monitored noninvasively by FLI using the IVIS Spectrum imaging system (PerkinElmer Life Science, Waltham, MA, USA). Images acquisition and measurements were performed using the Living Image 4.3 software (PerkinElmer). Mice were anesthetized using 1–3% isoflurane (Abbott Laboratories, Abbott Park, IL) and imaged at 0, 2, 4, and 24 h postadministration. Mice were maintained with water ad libitum and hydrogel during the experimental procedure. Mice were then euthanized at 25 h postadministration and major organs (lung, brain, liver, heart, bone from ribs, muscle from leg, kidney, digestive system, pancreas, and spleen) were excised and imaged by ex vivo FLI. The signal emitted by the fluorescent-labeled BP-EVs was detected and digitalized using the software Living Image 4.7.3 as a pseudo-color overlay onto a grey-scale image of the animal or excised tissue. Fluorescent signal of regions of interest was quantified as radiant efficiency.

Statistical Analysis: Data were reported as mean ± standard error of mean (SEM), otherwise specified. Data are derived from at least three biological replicates in all the experiments. Log2 transformation of data was performed by the software GraphPrism version 8.4.3. Gene

Ontology (GO) analysis for comparison of BP-EVs proteomes with human circulating EVs proteomes was performed with PANTHER version 16.0. List of proteins identified from human circulating EVs isolated by ultracentrifugation with sucrose cushion was obtained from a previously published work of the authors.[40] Further categorization of membrane proteins was performed by using in-house macro software or by performing functional enrichment analysis with the open-source specialized software FunRich version 3.1.4. Significance was assessed by parametric ANOVA or by nonparametric Kruskal Wallis with a minimum significance level $p < 0.05$. Statistical significance was indicated as: $*p < 0.05$ (parametric), $**p < 0.001$ (parametric), $\#p < 0.05$ (nonparametric), otherwise specified in the specific figure captions. GraphPad Prism version 8.4.3 was used for statistical analyses and for creating and rendering of data plots. Figures were assembled for the final version by using Illustrator 2020 software (Adobe, CA, USA).

Supporting Information

Supporting Information is available from the Wiley Online Library or from the author.

Acknowledgements

The authors sincerely thank Gemma Plaza, oenologist at the Castell del Remei winery in Penelles, Lleida, Spain and Juan Carlos Blanco, production manager at Mahou San Miguel in Alovera, Madrid, Spain for their kind and altruistic help on the obtention of their respective industry by-product samples. The authors also thank Dr. Hector Peinado and his research group at the National Center for Oncology Research (CNIO) in Madrid (Spain) for their support on the morphometric characterization of BP-EVs. Support for this work was provided by the Research and Education Council of the Community of Madrid, Spain (2018-T1/BIO-10633), Ministry of Science and Innovation, Spain (PID2020-114885RB-C21) and a FIS project by Carlos III Institute of Health (ISCIII), Spain (PI20/00623). A.S. acknowledges a grant from the Talento Program 2018 of the Community of Madrid. X.G.-P. acknowledges grants from Sara Borrell postdoctoral program (CD19/00243) and Miguel Servet tenure track program (CP21/00096) of the Instituto de Salud Carlos III (ISCIII, Spain), respectively awarded on the 2019 and 2021 calls under ISCIII-Health Strategy Actions [These grants are cofunded with European Union Funds (ISCIII Miguel Servet Program 2021 is cofunded by Fondo Social Europeo Plus, FSE+)]. M.V.C. acknowledges a Miguel Servet program contract (CPII20/00007). C.L.'s Ph.D. was funded by the Regional Ministry of Science, Universities and Innovation of the Community of Madrid and the European Social Fund for the recruitment of predoctoral researchers (PEJD-2019-PRE/BIO-16475). IRBLLEIDA and X.G.-P. are co-funded by CERCA Program/Generalitat de Catalunya.

Conflict of Interest

CL, EV, XG-P. & AS are inventors in a European patent application filed by the non-profit public research institutions: Institute of Research in Health Pere Virgili (IISPV), IMDEA Food & Health Sciences and CIBERSAM-ISCIII. The referred patent covers the obtention and any potential application(s) of BP-EVs obtained from industrial residues of fermented beverages, fermented dairy products and fermented plant-based products.

Author Contributions

C.L., X.G.-P., and A.S. performed isolation of BP-EVs, morphometric & ultrastructural characterization, sample processing for systems biology studies, proteomics experiments, and analysis of data. M.L. and C.L. performed in vitro studies. C.L., M.V.C., L.C., S.F., X.G.-P., and A.S. performed in vivo studies. C.L., M.J., and N.M.-M. performed sample processing, lipidomics, and data analysis. C.L., E.V., X.G.-P., and A.S. wrote the manuscript. C.L., X.G.-P., and A.S planned the experiments. X.G.-P. and A.S. conceived the study, obtained samples, obtained competitive funds, and supervised the project. All authors have read and approved the final version of the manuscript for submission.

Data Availability Statement

The proteomics data that support the findings of this study are openly available through the specialized repository PRIDE (https://www.ebi.ac.uk/pride/) with the following identifier: PXD025780. The Lipidomics data that support the findings of this study are openly available through the specialized repository MetaboLights (https://www.ebi.ac.uk/metabolights/index) with the following identifier: MTBLS2801. The rest of data generated remain at full disposition upon reasonable request.

Keywords

circular economy, extracellular vesicles, food industry by-products, lipidomics, mass spectrometry, nanocarriers, proteomics

Received: March 8, 2022
Revised: March 29, 2022
Published online: April 21, 2022

[1] L. Margolis, Y. Sadovsky, *PLoS Biol.* **2019**, *17*, e3000363.
[2] G. Raposo, W. Stoorvogel, *J. Cell Biol.* **2013**, *200*, 373.
[3] X. Gallart-Palau, A. Serra, S. K. Sze, *Mol. Neurodegener.* **2016**, *11*, 41.
[4] L. M. Doyle, M. Z. Wang, *Cells* **2019**, *8*, 727.
[5] M. Malloci, L. Perdomo, M. Veerasamy, R. Andriantsitohaina, G. Simard, M. C. Martínez, *Antioxid. Redox Signaling* **2019**, *30*, 813.
[6] W. Meng, C. He, Y. Hao, L. Wang, L. Li, G. Zhu, *Drug Delivery* **2020**, *27*, 585.
[7] P. Gangadaran, B.-C. Ahn, *Pharmaceutics* **2020**, *12*, 442.
[8] K. Adlerz, D. Patel, J. Rowley, K. Ng, T. Ahsan, *Stem Cell Res.* **2020**, *48*, 101978.
[9] P. Gangadaran, C. M. Hong, J. M. Oh, R. L. Rajendran, S. Kalimuthu, S. H. Son, A. Gopal, L. Zhu, S. H. Baek, S. Y. Jeong, S.-W. Lee, J. Lee, B.-C. Ahn, *Front. Pharmacol.* **2018**, *9*, 817.
[10] P. Pérez-Bermúdez, J. Blesa, J. M. Soriano, A. Marcilla, *Eur. J. Pharm. Sci.* **2017**, *98*, 40.
[11] E. A. Kang, H. I. Choi, S. W. Hong, S. Kang, H. Y. Jegal, E. W. Choi, B. S. Park, J. S. Kim, *Biomedicines* **2020**, *8*, 522.
[12] P. Akuma, O. D. Okagu, C. C. Udenigwe, *Front. Sustainable Food Syst.* **2019**, *3*, 23.
[13] G. Moraga, S. Huysveld, F. Mathieux, G. A. Blengini, L. Alaerts, K. Van Acker, S. de Meester, J. Dewulf, *Resour. Conserv. Recycl.* **2019**, *146*, 452.
[14] F. Girotto, L. Alibardi, R. Cossu, *Waste Manag.* **2015**, *45*, 32.
[15] R. E. Veerman, L. Teeuwen, P. Czarnewski, G. Güclüler Akpinar, A. Sandberg, X. Cao, M. Pernemalm, L. M. Orre, S. Gabrielsson, M. Eldh, *J. Extracell. Vesicles* **2021**, *10*, e12128.
[16] H. Sunshine, M. L. Iruela-Arispe, *Curr. Opin. Lipidol.* **2017**, *28*, 408.
[17] T. Skotland, K. Sandvig, A. Llorente, *Prog. Lipid Res.* **2017**, *66*, 30.
[18] G. Van Meer, D. R. Voelker, G. W. Feigenson, *Nat. Rev. Mol. Cell Biol.* **2008**, *9*, 112.
[19] J. S. Brzozowski, H. Jankowski, D. R. Bond, S. B. McCague, B. R. Munro, M. J. Predebon, C. J. Scarlett, K. A. Skelding, J. Weidenhofer, *Lipids Health Dis.* **2018**, *17*, 211.
[20] F. Meier, A. D. Brunner, S. Koch, H. Koch, M. Lubeck, M. Krause, N. Goedecke, J. Decker, T. Kosinski, M. A. Park, N. Bache, O. Hoerning, J. Cox, O. Räther, M. Mann, *Mol. Cell Proteomics* **2018**, *17*, 2534.

[21] C. G. Vasilopoulou, K. Sulek, A.-D. Brunner, N. S. Meitei, U. Schweiger-Hufnagel, S. W. Meyer, A. Barsch, M. Mann, F. Meier, *Nat. Commun.* **2020**, *11*, 331.
[22] S. Mathivanan, C. J. Fahner, G. E. Reid, R. J. Simpson, *Nucleic Acids Res.* **2012**, *40*, D1241.
[23] H. Kalra, R. J. Simpson, H. Ji, E. Aikawa, P. Altevogt, P. Askenase, V. C. Bond, F. E. Borras, X. Breakefield, V. Budnik, E. Buzas, G. Camussi, A. Clayton, E. Cocucci, J. M. Falcon-Perez, S. Gabrielsson, Y. S. Gho, D. Gupta, H. C. Harsha, A. Hendrix, A. F. Hill, J. M. Inal, G. Jenster, E. M. Kramer-Albers, S. K. Lim, A. Llorente, J. Lotvall, A. Marcilla, L. Mincheva-Nilsson, I. Nazarenko, et al., *PLoS Biol.* **2012**, *10*, e1001450.
[24] T. A. Reinhardt, J. D. Lippolis, B. J. Nonnecke, R. E. Sacco, *J. Proteomics* **2012**, *75*, 1486.
[25] S. Keerthikumar, D. Chisanga, D. Ariyaratne, H. Al Saffar, S. Anand, K. Zhao, M. Samuel, M. Pathan, M. Jois, N. Chilamkurti, L. Gangoda, S. Mathivanan, *J. Mol. Biol.* **2016**, *428*, 688.
[26] B. Pieters, O. Arntz, M. Bennink, M. Broeren, A. Caam, M. Koenders, P. Lent, W. Berg, M. de Vries, P. Kraan, F. A. J. Loo, *PLoS One* **2015**, *10*, e0121123.
[27] A. Stensballe, T. Bennike, *J. Extracell. Vesicles* **2014**, *3*, 27.
[28] H. Kim, M. Kim, K. Myoung, W. Kim, J. Ko, K. P. Kim, E. G. Cho, *Int. J. Mol. Sci.* **2020**, *21*, 8076.
[29] E. Woith, G. Fuhrmann, M. F. Melzig, *Int. J. Mol. Sci.* **2019**, *20*, 5695.
[30] K. Trajkovic, C. Hsu, S. Chiantia, L. Rajendran, D. Wenzel, F. Wieland, P. Schwille, B. Brügger, M. Simons, *Science* **2008**, *319*, 1244.
[31] H. S. Lee, I. C. Boulton, K. Reddin, H. Wong, D. Halliwell, O. Mandelboim, A. R. Gorringe, S. D. Gray-Owen, *Infect. Immun.* **2007**, *75*, 4449.
[32] M. J. Bruno, R. Rusinova, N. J. Gleason, R. E. KoeppeII, O. S. Andersen, *Faraday Discuss.* **2013**, *161*, 461.
[33] P. R. Odgren, L. W. HarvieJr, E. G. Fey, *Proteins* **1996**, *24*, 467.
[34] H. Shao, H. Im, C. M. Castro, X. Breakefield, R. Weissleder, H. Lee, *Chem. Rev.* **2018**, *118*, 1917.
[35] M. L. Marco, D. Heeney, S. Binda, C. J. Cifelli, P. D. Cotter, B. Foligné, M. Gänzle, R. Kort, G. Pasin, A. Pihlanto, E. J. Smid, R. Hutkins, *Curr. Opin. Biotechnol.* **2017**, *44*, 94.
[36] J. A. Tsatsaronis, S. Franch-Arroyo, U. Resch, E. Charpentier, *Trends Microbiol.* **2018**, *26*, 401.
[37] L. Macia, R. Nanan, E. Hosseini-Beheshti, G. E. Grau, *Int. J. Mol. Sci.* **2019**, *21*, 107.
[38] M. Kang, V. Jordan, C. Blenkiron, L. W. Chamley, *J. Extracell. Vesicles* **2021**, *10*, e12085.
[39] D. E. Murphy, O. G. de Jong, M. Brouwer, M. J. Wood, G. Lavieu, R. M. Schiffelers, P. Vader, *Exp. Mol. Med.* **2019**, *51*, 32.
[40] X. Gallart-Palau, A. Serra, A. S. W. Wong, S. Sandin, M. K. P. Lai, C. P. Chen, O. L. Kon, S. K. Sze, *Sci. Rep.* **2015**, *5*, 14664.
[41] A. N. Böing, E. van der Pol, A. E. Grootemaat, F. A. W. Coumans, A. Sturk, R. Nieuwland, *J. Extracell. Vesicles* **2014**, *3*, 23430.
[42] X. Gallart-Palau, A. Serra, Y. Hase, C. F. Tan, C. P. Chen, R. N. Kalaria, S. K. Sze, *Brain Pathol.* **2019**, *29*, 593.
[43] C. Pizarro, I. Arenzana-Rámila, N. Pérez-del-Notario, P. Pérez-Matute, J.-M. González-Sáiz, *Anal. Chem.* **2013**, *85*, 12085.
[44] I. Pradas, K. Huynh, R. Cabré, V. Ayala, P. J. Meikle, M. Jové, R. Pamplona, *Front. Physiol.* **2018**, *9*, 1165.
[45] J. M. Castro-Perez, J. Kamphorst, J. DeGroot, F. Lafeber, J. Goshawk, K. Yu, J. P. Shockcor, R. J. Vreeken, T. Hankemeier, *J. Proteome Res.* **2010**, *9*, 2377.
[46] I. Pradas, S. Rovira-Llopis, A. Naudí, C. Bañuls, M. Rocha, A. Hernandez-Mijares, R. Pamplona, V. M. Victor, M. Jové, *Sci. Rep.* **2019**, *9*, 16033.
[47] X. Gallart-Palau, X. Guo, A. Serra, S. K. Sze, *Alzheimer's Res. Ther.* **2020**, *12*, 54.